Electromagnetic Wave Emission from Intrinsic Josephson Junction Stacks: A Review of Theory and Simulation

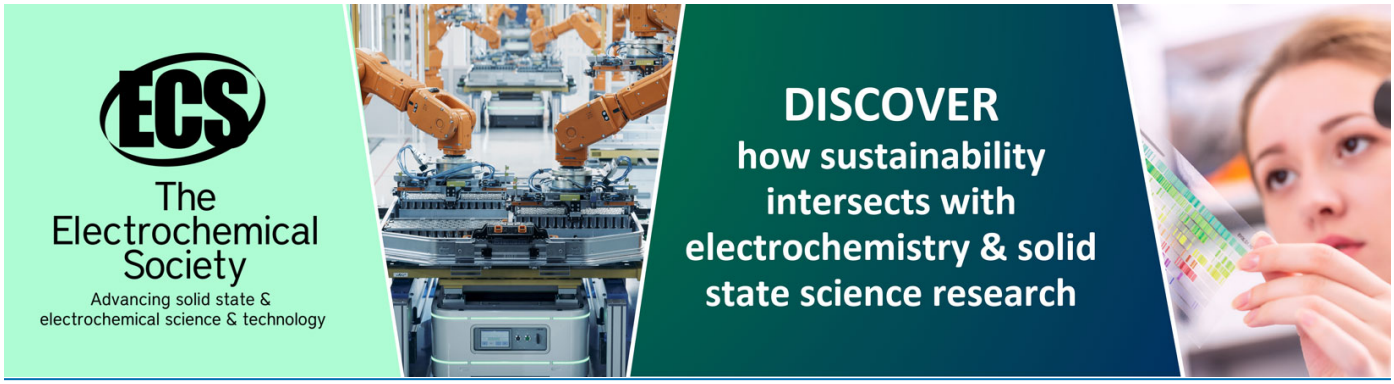

Journal of Physics: Conference Series **393** (2012) 012013 doi:10.1088/1742-6596/393/1/012013

Electromagnetic Wave Emission from Intrinsic Josephson Junction Stacks: A Review of Theory and Simulation

M Machida[1], Y Ota[2], T Koyama[3], and H Matsumoto[3]

[1] CCSE, Japan Atomic Energy Agency, 6-9-3 Higashi-Ueno Taito-ku, Tokyo, 110-0015, Japan
[2] Riken
[3] Institute for Materials Research, Tohoku University, 2-1-1 Katahira Aoba-ku, Sendai, 980-8577, Japan

E-mail: machida.masahiko@jaea.go.jp, otayuki@riken.go.jp, tkoyama@imr.tohoku.ac.jp, matumoto@ldp.phys.tohoku.ac.jp

Abstract.

We review theoretical and numerical research developments in intrinsic Josephson junctions in terms of spontaneous THz electromagnetic-wave emission and report our recent multi-scale simulation scheme to further enhance the radiation power. Starting with theoretical treatments on the couplings among the stacked Josephson junctions, we reveal that solitonic excitation is essential for large spontaneous emission. Finally, we propose an experimental setup, in which an intrinsic Josephson junction is enwrapped by the dielectric materials and reveal that radiation power enhancement occurs by tunning the dielectricity.

1. Introduction

The discovery of clear THz emission from layered High-Tc cuprate $Bi_2Sr_2CaCu_2O_{8-\delta}$ (Bi-2212) [1] was a great mileston for the community which had intensively studied intrinsic Josephson junctions (IJJ's) and related issues. The experimental observation has triggered new types of theoretical and numerical studies on IJJ's. For example, the connection of junctions with environmental vacuum has been not a primary issue but just a concerning one in the previous studies, while the connection mismatch is now a central one [2] to understand the emission mechanism and enhance the radiation power. In addition, although the magnetic field application has been long regarded to be essential for the spontaneous emission, the cavity resonance together with AC Josephson effect is now recognized as an promising mechanism than the resonant vortex flow [3].

Before the discovery of the zero-field emission by Ozyuzer et al., [1] the IJJ community has concentrated on the coupling between neighboring junctions and established two kinds of couplings. One of them is called inductive coupling, which arises from incomplete screening of the penetrated magnetic field within an atomic-scale junction [4],[5]. It can be theoretically characterized by the ratio of the magnetic field screening length to the single junction thickness. Then, the coupling strength is found to be quite large, since the magnetic field screening length extends over thousands of junctions. The capacitive coupling is its counterpart for the electric field [6],[7]. It similarly comes from incomplete screening of the induced electric field

within a superconducting layer [7]. The electric field screening length is comparable to the superconducting layer thickness, and the coupling is much weaker than the inductive coupling. However, the capacitive coupling is a unique one, which emerges only for atomic-scale junction stacks like IJJ's. It has an important role in small-scale IJJ's with no application of the magnetic field. In Section II, we present a theoretical review on both the couplings.

The theoretical framework studing the THz radiation from IJJ's is basically grounded on the superconducting phase dynamics. The dynamical action of the superconducting phase was derived from the microscopic treatment on the Cooper-pair Josephson tunneling in IJJ's [8]. Both the couplings are naturally involved in the dynamical action. The inductive coupling is known to bring about the cavity resonance. It occurs when the cavity mode frequency matches with the Josephson frequency given by the applied voltage. Theoretically, the resonance is described by the equation formulating the in-plane spatial variation of the superconducting phase together with the edge boundary condition. The correspondent equation is the coupled sine-Gordon equation, which has been intensively investigated by IJJ community. Since the equation is nonlinear and several junctions are nonlinearly coupled, numerical simulation has been regarded as a primary theoretical tool. In Section III, we briefly present the latest numerical simulation techniques [2]. The simulation area includes not only internal area of IJJ but also external one surrounding the junction. Such a technical extention is required to correctly study the emission mechanism and examine the radiation power enhancement. We emphasize that the technique offers a new tool to examine performance as an emitter in not only IJJ's but also the conventional Josephson junction.

The electromagnetic wave radiation occurs, when both the electric and the magnetic fields are excited inside the junction. Normally, the AC electric field is uniformly excited in the voltage state without magnetic field. Then, the Josephson relation gives the relation between the applied voltage and AC frequency. This implies that DC to AC conversion always occurs in the voltage state of Josephson junctions. However, it has been well-known that the radiation power caused by such a simple conversion is mostly quite weak. On the other hand, in the observed large THz emission, the frequency is uniquely given by the cavity resonance frequency [1],[9],[10]. This clearly indicates that the cavity resonance causes to enhance the Josephson AC oscillation and efficiently transport the excitation power into the emitted wave. Namely, the cavity resonance excites AC magnetic field component characterized by the spatial variation of the superconducting phase. It has been well-known that such a phase variation is generally brought about by vortices and other solitonic excitations, i.e., nonlinear localized modes. Thus, the interest is whether or not solitonic excitation really emerges at the cavity resonance frequency, and if it does, which type of solitonic mode is then excited. In Section IV, we reveal the solitonic excitation form at the cavity resonance frequencies from the numerical simulation result.

2. Theory of Couplings in IJJ's

In this section, we briefly review the theoretical developments on IJJ's. The most important development in this field is the establishement of the couplings between neighboring junctions, since the couplings cause collective features unique for IJJ's. We explain two coupling mechanisms from an effective action of the superconducting phase. It is interesting to say that both the two couplings can be naturally obtained from a theoretical requirment that the superconducting phase dynamics is governed by the gauge invariance.

2.1. Microscopic Model

We begin with a microscopic description for the stacked IJJ schematically depicted in Fig.1. In Bi-2212, we regard double CuO_2 planes as a single superconducting layer whose thickness $s \sim 3$ $\mathring{A}$ and other block layers as an insulating layer $D \sim 12$ $\mathring{A}$. It is well-known in Bi-2212 that c-axis transport is given by the quasi-particle and Cooper pair tunneling between neighboring

superconducting layers via the insulating one. The Cooper pair tunneling occurs only below the superconducting transition temperature.

In the present microscopic model, we examine a case, in which the current is biased only parallel to c-axis and the magnetic field is applied only parallel to the junction plane as shown in Fig.1. Namely, the presence of pancake types of vortices are not taken into account. Extending the BCS model for a single tunneling-junction [11] into IJJ stack, the system's partition function is given by the following imaginary-time functional integral over the Grassman fields, $\hat{\psi}_{\sigma\ell}$, $\psi_{\sigma\ell}$, for electrons, the gauge fields φ_ℓ, $\mathbf{A}_\ell$, $A^z_{\ell+1,\ell}$, and the auxiliary field corresponding to the superconducting order parameter, Δ_ℓ, where ℓ is the layer index and the z-component of the vector potential is defined on the link as $A^z_{\ell+1,\ell} = \int_\ell^{\ell+1} dz A^z$,

$$Z = \prod_\ell \int \mathcal{D}\bar{\psi}_{\sigma\ell}\mathcal{D}\psi_{\sigma\ell}\mathcal{D}\mathbf{A}_\ell\mathcal{D}A^z_{\ell+1,\ell}\mathcal{D}\varphi_\ell\mathcal{D}\Delta_\ell \mathrm{e}^{-\frac{1}{\hbar}S[\bar{\psi}_{\sigma\ell},\psi_{\sigma\ell},\mathbf{A}_\ell,A^z_{\ell+1,\ell},\varphi_\ell,\Delta_\ell]}, \tag{1}$$

where, S is the Euclidian action defined as $S = S_{\mathrm{matter}} + S_{\mathrm{field}}$ whose expressions are given as

$$S_{\mathrm{matter}} = \sum_\ell \int_0^{\beta\hbar} \mathrm{d}\tau \int \mathrm{d}\mathbf{r}[\frac{|\Delta_\ell|^2}{g} + \bar{\psi}_{\sigma\ell}(\mathbf{r},\tau)(\hbar\partial_\tau + \mathrm{i}e\varphi_\ell)\psi_{\sigma\ell}(\mathbf{r},\tau) + \bar{\Delta}_\ell\psi_{\downarrow\ell}\psi_{\uparrow\ell} + \Delta_\ell\bar{\psi}_{\uparrow\ell}\bar{\psi}_{\uparrow\ell}$$

$$-\bar{\psi}_{\sigma\ell}(\mathbf{r},\tau)\Big(\frac{\hbar^2}{2m}(\nabla - \mathrm{i}\frac{e}{\hbar c}\mathbf{A}_\ell)^{\mathbf{2}} + \mu_\ell\Big)\psi_{\sigma\ell}(\mathbf{r},\tau) + (\mathbf{T}_{\ell+\mathbf{1},\ell}\mathrm{e}^{\frac{\mathbf{e}}{\hbar\mathbf{c}}\mathbf{A}^{\mathbf{z}}_{\ell+\mathbf{1},\ell}}\bar{\psi}_{\sigma\ell+\mathbf{1}}\psi_{\sigma\ell} + \mathrm{c.c})\Big], \tag{2}$$

and

$$S_{\mathrm{field}} = \sum_\ell \int_0^{\beta\hbar} \mathrm{d}\tau \int \mathrm{d}\mathbf{r}\frac{D}{8\pi}\Big(\epsilon_c {E^z_{\ell+1,\ell}}^2 + {B^x_{\ell+1,\ell}}^2 + {B^y_{\ell+1,\ell}}^2\Big), \tag{3}$$

where, $T_{\ell+1,\ell}$ is the tunneling matrix element between ℓth and $(\ell+1)$th superconducting layers, $E^z_{\ell+1,\ell}$ is the electric field ($\equiv \frac{1}{cD}\frac{\partial A^z_{\ell+1,\ell}}{\partial\tau} - \frac{\varphi_{\ell+1}-\varphi_\ell}{D}$) along the z-axis, ϵ_c is the dielectric constant of the insulating barriers, and $B^x_{\ell+1,\ell}$ ($\equiv \frac{1}{D}\frac{A^z_{\ell+1,\ell}}{\partial y} - \frac{A^y_{\ell+1}-A^y_\ell}{D}$) and $B^y_{\ell+1,\ell}$ ($\equiv \frac{A^x_{\ell+1}-A^x_\ell}{D} - \frac{1}{D}\frac{A^z_{\ell+1,\ell}}{\partial x}$) are the magnetic fields parallel to the junction plane.

Following the standard technique to integrate out the fermion degree of freedom together with reasonable approximations, we have the following effective action,

$$S_{\mathrm{eff}} = \sum_\ell \int_0^{\beta\hbar} \mathrm{d}\tau \int \mathrm{d}\mathbf{r}_{||}\Big[\frac{D}{8\pi}\Big(\epsilon_c {E^z_{\ell+1,\ell}}^2 + {B^x_{\ell+1,\ell}}^2 + {B^y_{\ell+1,\ell}}^2\Big) + msn_s {v_s^\ell}^{||2} + \frac{s}{8\pi\mu_f^2}(\frac{\phi_0}{2\pi c}\frac{\partial\theta_\ell}{\partial\tau} + \varphi_\ell)^2$$

$$+ Jcos P_{\ell+1,\ell}(\tau,\mathbf{r}_{||})\Big] + \sum_\ell \int_0^{\beta\hbar}\mathrm{d}\tau\int_0^{\beta\hbar}\mathrm{d}\tau'\int\mathrm{d}\mathbf{r}_{||}\Big[(-\alpha(\tau-\tau')\cos(\frac{P_{\ell+1,\ell}(\tau,\mathbf{r}_{||}) - P_{\ell+1,\ell}(\tau',\mathbf{r}_{||})}{2}\Big], \tag{4}$$

where $\mu_f \equiv \sqrt{\frac{\lambda_{\mathrm{TF}}^2}{4\pi\epsilon}}$ is a constant related to the Thomas-Fermi screening length λ_{TF}, s is the thickness of the superconducting layers, n_s is the superfluid density, and $P_{\ell+1,\ell}$ and ${v_s}^{||}_\ell$ are, respectively, the gauge-invariant phase difference and superfluid velocity defined as $P_{\ell+1,\ell} \equiv \theta_{\ell+1} - \theta_\ell - \frac{2\pi}{\phi_0}A^z_{\ell+1,\ell}$ and ${v_s}^{||}_\ell \equiv \frac{\hbar}{2m}(\nabla_{||}\theta_\ell - \frac{2\pi}{\phi_0}\mathbf{A}^{||}_\ell)$. In obtaining Eq.(4), we use a local approximation for the integral kernels associated with the intra-layer current, charge fluctuation, and Cooper pair tunneling current. Consequently, msn_s, $\frac{s}{8\pi\mu_f^2}$, J are local and constant coefficients [8]. These approximations are valid for the low energy dynamics, with which the tunneling process is relevant. On the other hand, the integral kernels, $\alpha(\tau-\tau')$ in Eq.(4) describes the frequency-dependent quasi-particle tunneling, which brings about the dissipation current proportional to the time derivative of the gauge invariant phase difference with a dissipation parameter $\beta \equiv \frac{4\pi\sigma\lambda_c}{\sqrt{\epsilon_c}c}$. The form is equivalent with the Caldeira-Leggett's action [8]. See Ref. [8] for the details of the discussion.

2.2. Dynamical Equations and Couplings

From the action Eq.(4), we can derive the following coupled equations for the gauge-invariant phase difference $P_{\ell+1,\ell}$ and the charge density ρ_ℓ,

$$\frac{\epsilon_c\phi_0}{2\pi c^2 D}\frac{\partial^2 P_{\ell+1,\ell}}{\partial t^2}+\frac{4\pi}{cD}(\epsilon_c\mu_f^2-\lambda_{ab}^2)(\frac{\partial\rho_{\ell+1}}{\partial t}-\frac{\partial\rho_\ell}{\partial t})-\frac{4\pi}{c}\frac{\lambda_{ab}^2}{sD}\beta(\frac{dP_{\ell+2,\ell+1}}{dt}+\frac{dP_{\ell,\ell-1}}{dt}-2\frac{dP_{\ell+1,\ell}}{dt})$$

$$-\frac{\phi_0}{2\pi D}\frac{\partial^2 P_{\ell+1,\ell}}{\partial x^2}+\frac{4\pi}{c}(sinP_{\ell+1,\ell}+\beta\frac{dP_{\ell+1,\ell}}{dt})-\frac{4\pi}{c}\frac{\lambda_{ab}^2}{sD}(sinP_{\ell+2,\ell+1}+sinP_{\ell,\ell-1}-2sinP_{\ell+1,\ell})=0, \quad (5)$$

$$\frac{\phi_0\epsilon_c}{2\pi cD}(\frac{\partial P_{\ell+1,\ell}}{\partial t}-\frac{\partial P_{\ell,\ell-1}}{\partial t})+\frac{4\pi\epsilon_c\mu_f^2}{D}(\rho_{\ell+1}+\rho_{\ell-1}-2\rho_\ell)=4\pi s\rho_\ell \quad (6)$$

We notice that Eq.(5) and (6) contains two parameters, which are the electric field screening length, μ_f and the magnetic field screening length in the in-plane direction, λ_{ab}. These parameters differ extremely, i.e., $\mu_f \ll \lambda_{ab}$. The terms including the coefficient λ_{ab} describe the inductive coupling between junctions [4],[5], while the counterparts for μ_f do the capacitive one [6],[7].

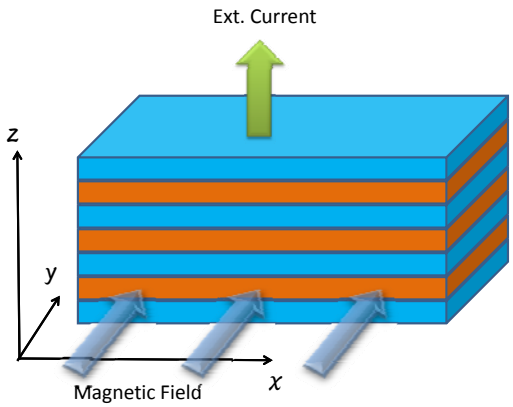

Figure 1. A schematic view for intrinsic Josephson junctions, in which the superconducting CuO_2 planes and insulating layers are alternatively stacked along z(c)-axis. The magnetic field and external current are supposed to be applied only in the layer parallel and perpendicular directions, respectively.

2.3. Dynamical Equations for Inductive and Capacitive Couplings

By elminating the terms including μ_f, i.e., $\mu_f \to 0$ in Eq.(5) and (6), and using the normalized units $t=t'/\omega_p, \omega_p=\frac{c}{\sqrt{\epsilon_c}\lambda_c}$ and $x=x'/\lambda_c$ we have the coupled sine-Gordon equation taking account of only the inductive coupling,

$$\frac{\lambda_{ab}^2}{sD}(\frac{\partial^2 P_{\ell+2,\ell+1}}{\partial t'^2}+\frac{\partial^2 P_{\ell,\ell-1}}{\partial t'^2}-2\frac{\partial^2 P_{\ell+1,\ell}}{\partial t'^2})+\frac{{\lambda_{ab}}^2}{sD}\beta(\frac{\partial P_{\ell+2,\ell+1}}{\partial t'}+\frac{\partial P_{\ell,\ell-1}}{\partial t'}-2\frac{\partial P_{\ell+1,\ell}}{\partial t'})$$

$$-\frac{\partial^2 P_{\ell+1,\ell}}{\partial x'^2}+\frac{{\lambda_{ab}}^2}{sD}(\sin P_{\ell+1,\ell}+\sin P_{\ell,\ell-1}-2\sin P_{\ell+1,\ell})-(\sin P_{\ell+1,\ell}+\beta\frac{\partial P_{\ell+1,\ell}}{\partial t'}+\frac{\partial^2 P_{\ell+1,\ell}}{\partial t'^2})=0. \quad (7)$$

This equation was initially examined by Sakai et al., in their analytical way [4], while a pioneering simulation on the Josephson vortex dynamics was made by Kleiner et al. [12] The main issue of the equation was the existence of the multiple plasma excitation modes propagating mainly along the in-plane direction, called the transverse plasma, and the resonant vortex dynamics with the multiple plasma modes [3]. The resonant vortex flow has been intensively investigated by several authors in the community. To our knowledge, the most surprising physics was the emergence of the in-phase locked vortex flow due to the resonance between the in-phase like propagating mode and flowing vortex lattice. The in-phase locked flux flow promises high-power radiation of THz wave [3]. However, there has been no clear evidence of such high-power radiation in the presence of the layer parallel magnetic field.

By assuming uniformity of the superconducting phase along the junction plane, all the terms originated from the inductive coupling vanish in Eq.(5) and Eq.(6), and a simple equation appears as follows.

$$\partial_{t'}^2 P_{\ell+1,\ell} + \beta \partial_{t'} P_{\ell+1,\ell} + \sin P_{\ell+1,\ell} = I/j_c$$
$$+\frac{\epsilon_c \mu_f^2}{sD}\Big[\sin P_{\ell+2,\ell+1} - 2\sin P_{\ell+1,\ell} + \sin P_{\ell,\ell-1}\Big] + \frac{\epsilon_c \mu_f^2}{sD}\beta\Big[\frac{dP_{l+2,l+1}}{dt'} - 2\frac{dP_{l+1,l}}{dt'} + \frac{dP_{l,l-1}}{dt'}\Big]. \quad (8)$$

This equation was firstly derived by Machida et al., through the micrscopic treatment [8]. We immediately notice that if one drops the third term in the right-hand side, then Eq.(8) coincides with Koyama-Tachiki model derived by their phenomenological treatment [6]. The model has been investigated initially by Machida et al., [7] and recently by Shukrinov et al., [13],[14]. The main physics of the model is the existence of the localized rotating mode, which has been intensively studied in nonlinear physics community motivated by a counter-intuitive concept, in which fully stable localized excitaions emerge even on non-integrable discrte lattice models like solitonic excitations [7],[13],[14].

3. Numerical Simulation Techniques for THz Radiation

In the previous section, we derived the general equations describing both the inductive and capacitive couplings. In this section, we present the latest numerical techniques to simulate the electromagnetic wave emission from IJJ's. The research target is further radiation power enhancement.

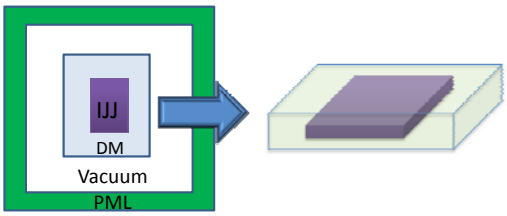

Figure 2. A schematic view for the simulation region to examine the THz radiation mechanism and the radiation power enhancement. The region are composed of IJJ, the surrounding vacuum, and the perfectly matched layer (PML). In the present case, it is noted that IJJ is enwrapped by a dielectric medium (DM) to improve the mismatch in the external radiation.

4. Multiscale Modeling for Electromagnetic Wave Emission

In addition to the coupled sine-Gordon Eq.(5) and (6), the EM fields in the dielectric medium or the vacuum outside the IJJ's device as schematically shown in Fig.2 is described by the Maxwell equations [2],

$$\frac{\epsilon(x,z)}{c}\partial_t E_x(x,z,t) = -\nabla_z B_y(x,z,t), \tag{9}$$

$$\frac{1}{c}\partial_t B_y(x,z,t) = \nabla_x E_z(x,z,t) - \nabla_z E_x(x,z,t). \tag{10}$$

where the dielectric constant $\epsilon(x,z)$ is chosen as $\epsilon(x,z) = \epsilon_D$ inside the dielectric medium or $\epsilon(x,z) = 1$ in the vacuum. An IJJ device is located in the region $-L_x/2 < x < L_x/2$, where L_x is the in-plane length in the x-direction. In this case, we apply the external current given as, $j_{\rm ext}(x,z) = j_{\rm ext}\theta(x+L_x/2)\theta(x-L_x/2)[\theta(-W_z/2-z)+\theta(z-W_z/2)]$, where $\theta(x)$ is the step function and the position $z = \pm W_z$ is chosen inside the electrodes.

In the present simulation, we solve Eqs.(5),(6),(9), and (10) in a finite box as shown in Fig.2, though the surrounding space is infinitely large. To avoid unphysical reflection of the EM waves at the artificial box boundary, we introduce the PML (perfectly matched layer) enwrapping the simulation box [2]. The PML is a fictitious layer that absorbs the outgoing EM waves without any reflection. In PML, the EM fields are decomposed, depending on the propagating directions. For example, B_y is decomposed into two components as $B_y = B_{yx} + B_{yz}$, where B_{yx} (B_{yz}) is the component propagating in the x (z) direction. The decomposed fields are assumed to obey the following quasi-Maxwell equations which bring about the rapid decrease for the decomposed fields,

$$\frac{1}{c}\partial_t E_{xz} = -\nabla_z B_y - \sigma_{xz}E_{xz}, \quad \frac{1}{c}\partial_t E_{zx} = \nabla_x B_y - \sigma_{zx}E_{zx}, \tag{11}$$

$$\frac{1}{c}\partial_t B_{yx} = \nabla_x E_z - \sigma_{yx}B_{yx}, \quad \frac{1}{c}\partial_t B_{yz} = -\nabla_z E_x - \sigma_{yz}B_{yz}, \tag{12}$$

where $E_{xz} = E_x$ and $E_{zx} = E_z$. The explicit expressions for the damping factors $\sigma_{\alpha\beta}$ used in this paper, which damp the EM waves propagating inside the PML, are given in Ref.[2].

Outside the IJJ device, the grid pitch is given as $\Delta_x = \Delta_z = 0.01\lambda_c \sim 2\mu$m (Bi-2212 IJJ's), since the wavelength of emitted EM waves is on the order of λ_c. On the other hand, the grid pitch in the interanl junction area is in a scale of λ_J, which is quite small compared to λ_c. In addition, it is noted that a mesa sample in which THz emission occurs has a thickness $D \sim 1\mu$m, that is, $D < \Delta_z$. To perform the calculations in such a real multiscale system, one needs an approximations in solving Eqs.(5),(6), and Eqs.(9),(10) simultaneously. Thus, we impose a coarse-grained condition at the junction edges that the EM field averaged over all the junctions along the z-direction is continuously connected to the EM field outside the IJJ's. This assumption was verified by a comparison with experimental observations. Moreover, it is noted that we treat IJJ's whose $N = 20$ junctions, applying the periodic boundary condition along the z-direction, though real mesas emitting EM waves contain thousands of junctions. The reason is that the system containing several hundreds of junctions is too large for the present numerical resource. One needs parallelization techniques to divide the box region as Fig.2 with keeping each PE's calculation cost equivalent. The parallelization is the future task. More details of the numerical scheme to solve the coupled dynamical equations (5),(6),(9), and (10) is given in Ref.[2].

5. Numerical results and discussions

Now, let us present the numerical simulation results. We perform various simulations for an IJJ device covered by a dielectric film of thickness $0.02\lambda_c$ and in-plane size $0.5\lambda_c$ as

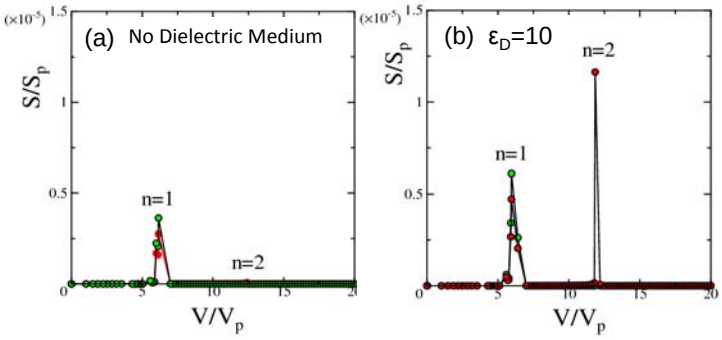

Figure 3. The simulation results for the applied voltage dependences of the radiation power in (a) no dielectric medium covered and (b) covered cases, in which the dielectric constant $\epsilon_D = 10$. The red and green circles denote the power in the directions [100] and [001], respectively.

schematically shown in Fig.2. The device parameter values are taken as $\frac{\epsilon_c \mu_f}{sD} = 0.1$, $\frac{\lambda_{ab}^2}{sD} = 10^4$, $\beta \equiv \sigma(\hbar\omega_p/2eDj_c) = 0.05$, and $\beta_L \equiv \sigma_L(\hbar\omega_p/2eDj_c) = 100$ with ω_p being the Josephson plasma frequency $\omega_p = c/\sqrt{\epsilon_c}\lambda_c$.

Figure 3 shows the voltage dependences of the power of the EM waves (Poynting vector) emitted in the two directions [100] and [001]. In these simulations, we take the value $\epsilon_D = 10$ for the dielectric constant of the covered dielectric medium, since a good impedance matching between the IJJ's and the outside space occurs, i.e., $\epsilon_D = \epsilon_c$. In the case of no dielectric medium, the emission peak can be observed only at $n = 1$ cavity mode excitation in an agreement with the observation by Ozyuzer et al., [1]. On the other hand, in the case covered by the dielectric medium, two peaks $n = 1$ and $n = 2$ cavity mode resonances are observed. Here, it is noted that $n = 1$ and $n = 2$ cavity resonances are, respectively, characterized by the relations as $V/V_p \sim \nu_1/\omega_p = \pi(\lambda_c/L) = 2\pi$ and $V/V_p \sim \nu_2/\omega_p = 2\pi(\lambda_c/L) = 4\pi$ with $V_p = \hbar\omega_p/2e$. Comparing between these figures, the peak intensity of the resonant modes is found to become larger in the presence of the dielectric cover. Then, we also check that AC EM fields excited by the Josephson oscillations penetrates well into the dielectric medium, that is, the impedance matching is improved in the system. It is also noticed that the enhancement of the $n = 2$ resonant peak is large compared with that of the $n = 1$ resonance peak and the emission from the $n = 2$ mode is directed mainly in the [100] direction, because the power in the [001] direction is negligibly small, which is expected in the dipole type of emission. To understand this unexpected increase in the peak intensity of the $n = 2$ mode, we plot a snapshot of the phase differences $P_{\ell+1,\ell}(x)$ in Fig.4(a). As seen in this figure, the phase differences exhibit an alternate structure along the c-direction as $\cdots = P_{2\ell+1,2\ell}(x,t) = -P_{2\ell,2\ell-1}(x,t)$. Such an alternate one has been also suggested at $n = 1$ cavity resonance in Refs. [15] and [16]. As seen in Fig.4(a), the spatial variation along the in-plane direction exhibits localized solitonic structures with π-phase shift, i.e., $0 \to \pi$ or $\pi \to 0$. In contrast, such solitonic variations are not at all observed except for the resonances at $n = 1$ and 2. From these results, one understands that the strong radiation comes from the excitation of solitonic modes.

In order to seek whether an optimum value of ϵ_D whose suitable choice leads to stronger emission or not, we examine the emission power variation by changing its value. Fig.4(b) shows the power of EM waves emitted from $n = 2$ resonant mode as a function of ϵ_D. From these results, one may expect that the optimum value of ϵ_D which leads to the strongest emission.

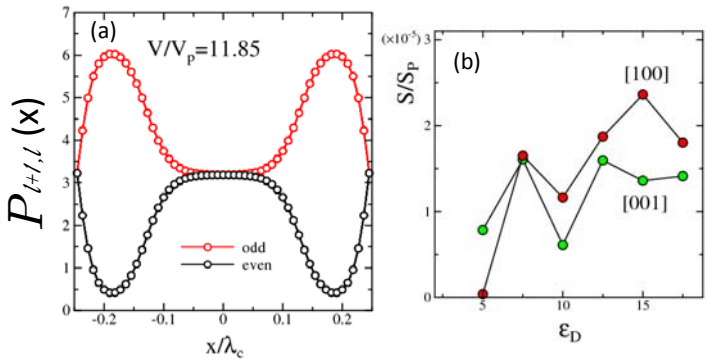

Figure 4. The simulation results for (a) the spatial profile snapshot of $P_{\ell+1,\ell}$ in the radiation state assigned as $n = 2$ and (b) the dielectric constant dependences of the radiation power.

6. Summary

We reviewed the theoretical framework for the intrinsic Josephson junction systems. Starting with the microscopic tunneling model, we reach the general equations of the superconducting phase and the charge density and derive approximate equations describing the inductive or capacitive coupling. Finally, we introduced the latest numerical scheme to examine the electromagnetic wave radiation in realistic situations and presented typical simulation results. An idea to enhance the radiation power was suggested together with the numerical confirmations.

Acknowledgments

The authors wish to acknowledge valuable discussions with K. Kadowaki, R. Kleiner, H-B. Wang, A. E. Koshelev, and Y. Shukrinov. M.M. was partially supported by Grant-in-Aid for Scientific Research from the Ministry of Education, Culture, Sports, Science and Technology of Japan (MEXT).

References

[1] Ozyuzer L, Koshelev A E, Kurter C, Gopalsami N, Li Q, Tachiki M, Kadowaki K, Yamamoto T, Minami H, Yamaguchi H, Tachiki T, Gray K E, Kwok W K, and Welp U, 2007 *Science* **318** 1291
[2] Koyama T, Matsumoto H, Machida M, Ota Y, 2011 *Supercond. Sci. Technol.* **24** 085007
[3] Machida M, Koyama T, and Tachiki M, 2000 *Physica* C **330** 85
[4] Sakai S, Bodin P, and Pedersen N F, 1993 *J. Appl. Phys.* **73** 2411
[5] Bulaevskii L N, Zamora M, Baeriswyl D, Beck H, and Clem J R, 1994 *Phys. Rev.* B **50** 12831
[6] Koyama T and Tachiki M, 1996 *Phys. Rev.* **B** 16183
[7] Machida M, Koyama T, and Tachiki M, 1999 *Phys. Rev. Lett.* **83** 4618
[8] Machida M, Koyama T, Tanaka A, and Tachiki M, 2000 *Physica* C **331** 85
[9] Tsujimoto M, Yamaki K, Deguchi K, Yamamoto T, Kashiwagi T, Minami H, Tachiki M, Kadowaki K, and Klemm R A, 2010 *Phys. Rev. Lett.* **105** 037005
[10] Wang H B, Gue'non S, Gross B, Yuan J, Jiang Z G, Zhong Y Y, Grünzweig M, Iishi A, Wu P H, Hatano T, Koelle D, and Kleiner R, 2010 *Phys. Rev. Lett.* **105** 057002
[11] Eckern U, Schön G, and Ambegaokar V, 1984 *Phys. Rev.* B **30** 6419
[12] Kleiner R, 1994 *Phys. Rev.* B **50** 6919
[13] Shukrinov Yu M and Mahfouzi F, 2007 *Phys. Rev. Lett.* **98** 157001
[14] Shukrinov Yu M, Hamdipour M, and Kolahchi M R, 2009 *Phys. Rev.* B **80** 014512
[15] Lin S and Hu X, 2008 *Phys. Rev. Lett.* **100** 247006.
[16] Koshelev A E, 2008 *Phys. Rev. B* **78** 174509